

Article

Anisotropy of Magnetic Susceptibility and Preferred Pore Orientation in Lava Flow from the Ijen Volcanic Complex, East Java, Indonesia

Fadhli Ramadhana Atarita ¹, Satria Bijaksana ^{1,*} , Nuresi Rantri Desi Wulan Ndari ¹, Aditya Pratama ¹ , Reyhan Fariz Taqwantara ¹, Silvia Jannatul Fajar ¹  and Fourier Dzar Eljabbar Latief ²

¹ Faculty of Mining and Petroleum Engineering, Institut Teknologi Bandung, Bandung 40132, Indonesia

² Faculty of Mathematics and Natural Science, Institut Teknologi Bandung, Bandung 40132, Indonesia

* Correspondence: satria@fi.itb.ac.id; Tel.: +62-816-617-228

Received: 30 March 2019; Accepted: 10 July 2019; Published: 11 July 2019



Abstract: Anisotropy of magnetic susceptibility (AMS) has been used in various studies related to interpreting the direction of lava flow, some of which have shown ambiguity with regard to the data generated. In this study, we explored an alternative option to support the aforementioned application, using lava flow type igneous rock samples from the Ijen Volcanic Complex, East Java, Indonesia. We have investigated the preferred rock pore orientations from micro-computed tomography (μ CT) images and quantified their directions. We then calculated their correlation with AMS data by calculating the angle between preferred pore orientation. The axis with the smallest gap to the preferred pore orientation of each sample was assumed to imply lava flow direction. Different lava flow direction preferences were obtained from different magnetic ellipsoids. Another important factor for consideration is the relative vertical position of the sampling site within a single lava flow unit. Only one out of five samples (ANY2) show good quantitative conformity between AMS data, preferred pore orientation, and topographical slope, despite these limitations. Our results point to a direction that seems to be correct and coherent on a physical basis. Additional research would likely clarify the issues involved. This encourages us to explore and work further in this field of research.

Keywords: anisotropy of magnetic susceptibility (AMS); preferred pore orientation; igneous rock; lava flow direction

1. Introduction

Anisotropy of magnetic susceptibility (AMS) is defined as the characteristic of a rock that has different values of magnetic susceptibility if measured by different angles or directions. This particular parameter has been used in previous studies, most commonly to determine lava flow direction [1–10]. However, the results of these studies are inconsistent: Some concluded that flow direction was parallel to the maximum susceptibility axis [1–4]; one study indicated that the intermediate susceptibility axis flow direction tended to be parallel [5]; another study [6] showed that there were differences in the characteristics between the end and toe of a lava flow. In addition, other studies concluded that AMS was not always reliable for indicating lava flow direction [6–9]. The study in reference [11] on Xitle lava in Mexico showed no correlation between lava flow direction and the maximum or intermediate susceptibility axes. These contradictory results could be accommodated by considering the local lava flow direction. Based on these inconsistencies, it is difficult to generalize statements regarding the correlation between AMS and lava flow direction [12]. Nevertheless, the correlation between AMS and lava flow direction is undeniable [13].

Hence there is a need to introduce another parameter to the equation that can facilitate interpreting lava flow direction using AMS data. In this study, we proposed pore orientation as an auxiliary parameter in lava flow direction interpretation. When pressure drops during rock formation, vesicles are formed, causing an increase in gas content inside magma under saturated conditions [14]. The trapped gas then diffuses from the newly-formed rock, forming empty space within it. By analyzing the preferred pattern of pore orientation, we can predict lava flow direction. The long-axis and inclination of vesicles/pores inside the rock can indicate the movement of lava at the time of rock formation [15]. Obstacles on the ground can disturb lava movement, causing tilting of flattened vesicles towards their source [16]. We analyzed lava flow direction using images of pores inside the specimens. The images were generated using the micro-computed tomography (μ CT) method, which has been applied for geoscience purposes in several studies [17–22].

The aim of our study was to identify alternatives in lava flow direction interpretation using AMS data, to specifically correlate AMS with the preferred pore orientation. Only a few studies have previously combined AMS and pores/vesicles analysis [9,23]. In this paper, we discuss our results correlating AMS data and pore orientation obtained from the μ CT images relevant to their implication on lava flow direction. This study is one of the first attempts to combine these two parameters in this context, which could be a new solution to the problem encountered in previous studies.

2. Samples and Measurements

2.1. Samples

We used five lava samples from five different outcrops in the Ijen Volcanic Complex, West Java, Indonesia (Figure 1), the outcrops of which have been the sites of previous research [24,25]. Identifying mineralogy, texture, geochemistry, and rock magnetic properties of lavas, which were resulted from Ijen Crater and Mount Anyar eruptions was performed in a previous study [25]. Four samples (ANY1, ANY2, ANY3, and ANY4) are products of Mount Anyar's eruption. Meanwhile, another sample (IJ1) was the product of Ijen Crater's eruption. The eruptions occurred about 2590 years ago [26]. The characteristics of all samples (based on reference [25]) are shown in Table 1.

Sample locations in the lava body were different. ANY1 and IJ4 were positioned relatively at the bottom part of the lava body, while others were found in the upper part. ANY3 and ANY4 were taken from the surface of the flow, while ANY2 was found relatively below them. No samples were taken from the middle part of the lava body, because usually samples from this zone are more compact with no visible vesicles. This sampling method was applied to investigate the effect of sample location in the lava body to the characteristics of anisotropy and pore distribution in the lava sample. In addition, outcrop sites have different slopes: IJ4 site had a slope ~20–25 degrees with northwest relative direction; ANY1, ANY2, ANY3, and ANY4 sites had directions relative to the northeast with ~35–40 degree slopes. Slope data were taken from the topography map created by the Geospatial Information Agency (Badan Informasi Geospasial, BIG) of the Republic of Indonesia. We converted the topography map to slope map using ArcGIS software (by ESRI, Redlands, CA, USA).

Lava samples obtained from the field were then prepared to form cylindrical cores, six of each (from now on will be referred as specimens) at the Faculty of Mining and Petroleum Engineering, Institut Teknologi Bandung. The dimension of each core was 2.5 cm in diameter and 2.2 cm in height. All specimens were used in magnetic susceptibility measurements. One specimen of each hand sample was used to generate a pore distribution image using the μ CT method.

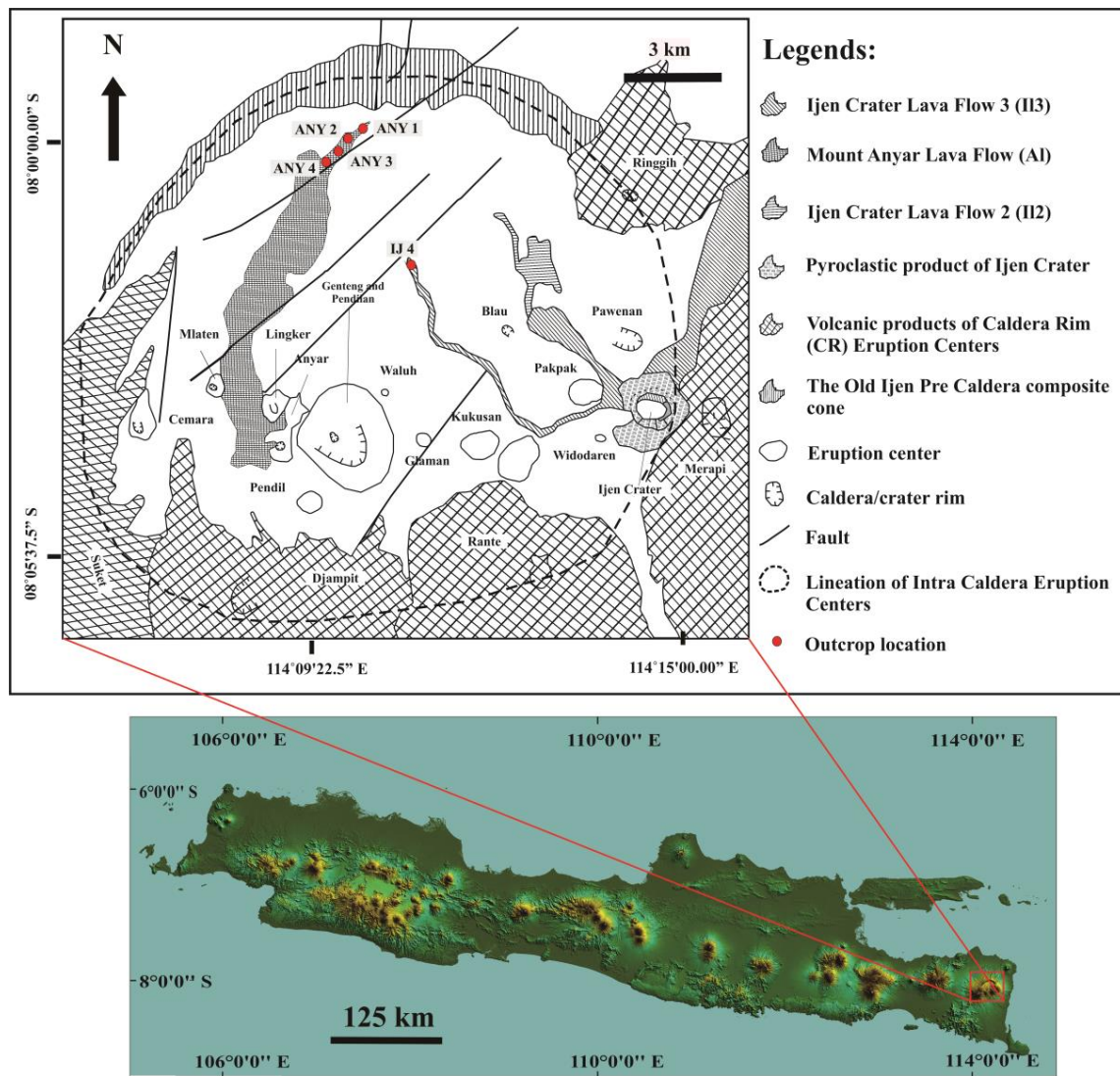


Figure 1. The Ijen Volcanic Complex map shows the distribution of volcanic products and eruption centers. Red dots indicate the sampling sites (modified from reference [25]).

Table 1. Magnetic and petrography data of the samples [25].

Sample	IJ4	ANY1	ANY2	ANY3	ANY4
Source	Ijen Crater	Mt. Anyar	Mt. Anyar	Mt. Anyar	Mt. Anyar
Lithology	Andesite Basaltic	Basalt	Basalt	Basalt	Basalt
Opaque mineral (%)	8	8	6	7	6
Predominant grain shape of opaque mineral	Subhedral, Granular	Subhedral, Prismatic	Subhedral, Prismatic	Subhedral, Prismatic	Subhedral, Prismatic
Vesicular/Porosity (%)	2	4	12	12	15
Saturation Field IRM (mT)	140	240	340	350	337
Curie Temperature (T_c) (°C)	-	-	-	~350 and ~550	-
M_{rs}/M_s	0.20	0.31	-	0.30	0.26
H_{cr}/H_c	2.81	1.78	-	1.21	1.98
Predominant Magnetic mineral	Titano-magnetite	Titano-magnetite	Titano-Magnetite	Titano-magnetite	Titano-magnetite
Predominant Magnetic Domain	PSD	PSD	PSD	PSD	PSD

Notes: M_{rs} = magnetic saturation remanence; M_s = saturation magnetization; H_{cr} = coercivity of remanent; H_c = coercive force.

2.2. Anisotropy of Magnetic Susceptibility

Magnetic susceptibilities of rocks can have different values, depending on their measurement direction. In a three-axis coordinate system, three principal magnetic susceptibilities exist: K_1 , K_2 , and K_3 , known as maximum susceptibility, intermediate susceptibility, and minimum susceptibility, respectively with K_m as their mean value ($K_m = (K_1 + K_2 + K_3)/3$). In an isotropic medium, these three susceptibilities are equal in magnitude. However, in an anisotropic medium, the magnitudes are different, with the relationship $K_1 > K_2 > K_3$. We also used the degree of anisotropy ($P\%$) defined as ratio between K_1 and K_3 , rationalized by 100% to determine a sample's anisotropy. P_j is a corrected anisotropy degree and defined as $P_j = \exp \sqrt{2[(\eta_1 - \eta_m)^2 + (\eta_2 - \eta_m)^2 + (\eta_3 - \eta_m)^2]}$ with $\eta_1 = \ln K_1$, $\eta_2 = \ln K_2$, $\eta_3 = \ln K_3$, and $\eta_m = \sqrt[3]{(\eta_1 \cdot \eta_2 \cdot \eta_3)}$.

Magnetic susceptibility measurements were conducted using a Bartington Susceptibility Meter MS2 instrument at the Faculty of Mining and Petroleum Engineering, Institut Teknologi Bandung. The measurements were carried out in six directions: Up-down (A1), north-south (A2), east-west (A3), north-east (A4), north-down (A5), and east-down (A6) modified from the original nine directions technique [27]. Each measurement was conducted in low-frequency (χ_{LF}), at 470 Hz [28,29]. For quality control, we conducted the measurements three times for each direction, and the standard deviation was no more than 2%.

2.3. Pore Orientation

Micro-computed Tomography (μ CT) imaging is based on X-ray tracing while passing through a medium. In this study, the imaging process was conducted using a Bruker MicroCT Scanning Devices—SkyScan 1173 instrument at the Faculty of Mathematics and Natural Sciences, Institut Teknologi Bandung. This method is not destructive, with no damage to the specimens. The device generates high energy X-ray beams that can penetrate high-density rocks. The principle of this device is based on X-ray attenuation when the radiation passes the specimen, where high density corresponds to high attenuation. This process allowed us to differentiate between the solid parts and pores of the sample using the gray threshold [30]. A previous study has shown that porosity measurement results obtained using the CT method were similar to the results obtained using conventional methods [31].

To produce a 3D image, the object is rotated inside the device and the measurements are taken at particular degrees with constant increments. The raw datasets obtained using the instrument are then reconstructed to create a whole image of the samples using NRecon software (by Bruker MicroCT). After reconstruction, the images were then filtered using BLOB3D software (by The High-Resolution X-ray Computed Tomography Facility at The University of Texas at Austin/UTCT) [32] to differentiate between the solid part—referred as matrix—and the pores within the specimens. The process was done by filtering the pores from the matrix using the grayscale filter. In general, pores have low grayscale values, while matrices have relatively higher values. After filtering, the pores can be observed. Black and greyish hues were representative of the solid parts and the pores, respectively. These filtered images were then analyzed using the Directionality plugin from ImageJ program (developed by Wayne Rasband as an open source software) [33] in order to identify the pores' preferred orientation. This plugin analyzed the structures, i.e., the pores, in the input images and computed a histogram of the structure's amount of directions. This histogram was calculated using either local gradients orientation method or Fourier components analysis. Local gradients orientation is a local method that calculates the image using a 5×5 Sobel filter to derive the local gradient orientations. Meanwhile, the Fourier components analysis uses Fourier transform to transform the images and computes the images' Fourier power spectra. The results from these two methods can automatically computed by the Directionality plugin. A preferred pore orientation was analyzed from the histograms and their respective rose diagrams.

3. Results

3.1. Magnetic Anisotropy Parameters

Table 2 shows the magnetic anisotropy parameters for all specimens. Samples from Mt. Anyar were more anisotropic than samples from Mt. Ijen Muda. T indicates the shape parameter of each specimens [34] and is defined as $T = (2\eta_2 - \eta_1 - \eta_3)/(\eta_1 - \eta_3)$. Positive value $T > 0$ means that the specimen has oblate shape while negative value $T < 0$ indicates prolate shape [35]. It is important to note that within the same sample, specimens might have either prolate or oblate shapes. From all specimens, only IJ4 had an overall positive value, indicating the sample has oblate shape (Figure 2), in contrast with ANY1, ANY2, and ANY3, which had overall negative value. Meanwhile, ANY4 had an equal number of positive and negative valued specimens.

Table 2. Magnetic anisotropy parameters for all specimens.

Sample	Specimen	K_m (SI)	T	L	F	P_j	$P\%$	$P\%_{mean}$
ANY1	ANY1_1	1.624×10^{-5}	-0.038	1.024	1.022	1.046	4.611	6.790
	ANY1_2	1.572×10^{-5}	-0.208	1.035	1.023	1.059	5.831	
	ANY1_3	1.590×10^{-5}	-0.209	1.040	1.026	1.067	6.678	
	ANY1_4	1.595×10^{-5}	0.010	1.040	1.041	1.083	8.302	
	ANY1_5	1.571×10^{-5}	-0.010	1.034	1.033	1.068	6.830	
	ANY1_6	1.578×10^{-5}	0.356	1.027	1.057	1.087	8.491	
ANY2	ANY2_1	0.954×10^{-5}	0.823	1.002	1.021	1.025	2.275	2.786
	ANY2_2	0.918×10^{-5}	-0.066	1.027	1.024	1.052	5.218	
	ANY2_3	0.903×10^{-5}	0.389	1.008	1.019	1.027	2.679	
	ANY2_4	1.980×10^{-5}	-0.856	1.015	1.001	1.018	1.629	
	ANY2_5	2.024×10^{-5}	-0.098	1.013	1.011	1.024	2.419	
	ANY2_6	2.007×10^{-5}	-0.748	1.022	1.003	1.027	2.497	
ANY3	ANY3_1	1.403×10^{-5}	-0.567	1.019	1.005	1.026	2.468	4.213
	ANY3_2	1.140×10^{-5}	-0.089	1.018	1.015	1.033	3.261	
	ANY3_3	1.329×10^{-5}	-0.542	1.020	1.006	1.027	2.563	
	ANY3_4	1.300×10^{-5}	0.353	1.019	1.041	1.062	6.078	
	ANY3_5	1.148×10^{-5}	-0.378	1.027	1.012	1.041	3.982	
	ANY3_6	1.140×10^{-5}	-0.442	1.049	1.019	1.072	6.928	
ANY4	ANY4_1	1.154×10^{-5}	0.337	1.012	1.024	1.037	3.590	4.528
	ANY4_2	1.130×10^{-5}	0.428	1.015	1.037	1.054	5.223	
	ANY4_3	1.220×10^{-5}	0.361	1.014	1.029	1.044	4.302	
	ANY4_4	0.954×10^{-5}	-0.010	1.018	1.017	1.035	3.541	
	ANY4_5	0.894×10^{-5}	-0.436	1.035	1.013	1.050	4.862	
	ANY4_6	0.933×10^{-5}	-0.356	1.038	1.018	1.058	5.652	
IJ4	IJ4_1	1.019×10^{-5}	-0.247	1.023	1.014	1.037	3.640	3.204
	IJ4_2	1.046×10^{-5}	0.687	1.007	1.040	1.051	4.739	
	IJ4_3	9.709×10^{-5}	0.638	1.005	1.025	1.033	3.076	
	IJ4_4	0.962×10^{-5}	0.470	1.008	1.023	1.033	3.194	
	IJ4_5	0.896×10^{-5}	0.433	1.005	1.014	1.020	1.897	
	IJ4_6	0.913×10^{-5}	0.690	1.004	1.023	1.029	2.675	

Notes: K_m = mean susceptibility; T = shape parameter; L = lineation; F = foliation; P_j = corrected degree of anisotropy; $P\%$ = degree of anisotropy; $P\%_{mean}$ = mean of degree of anisotropy.

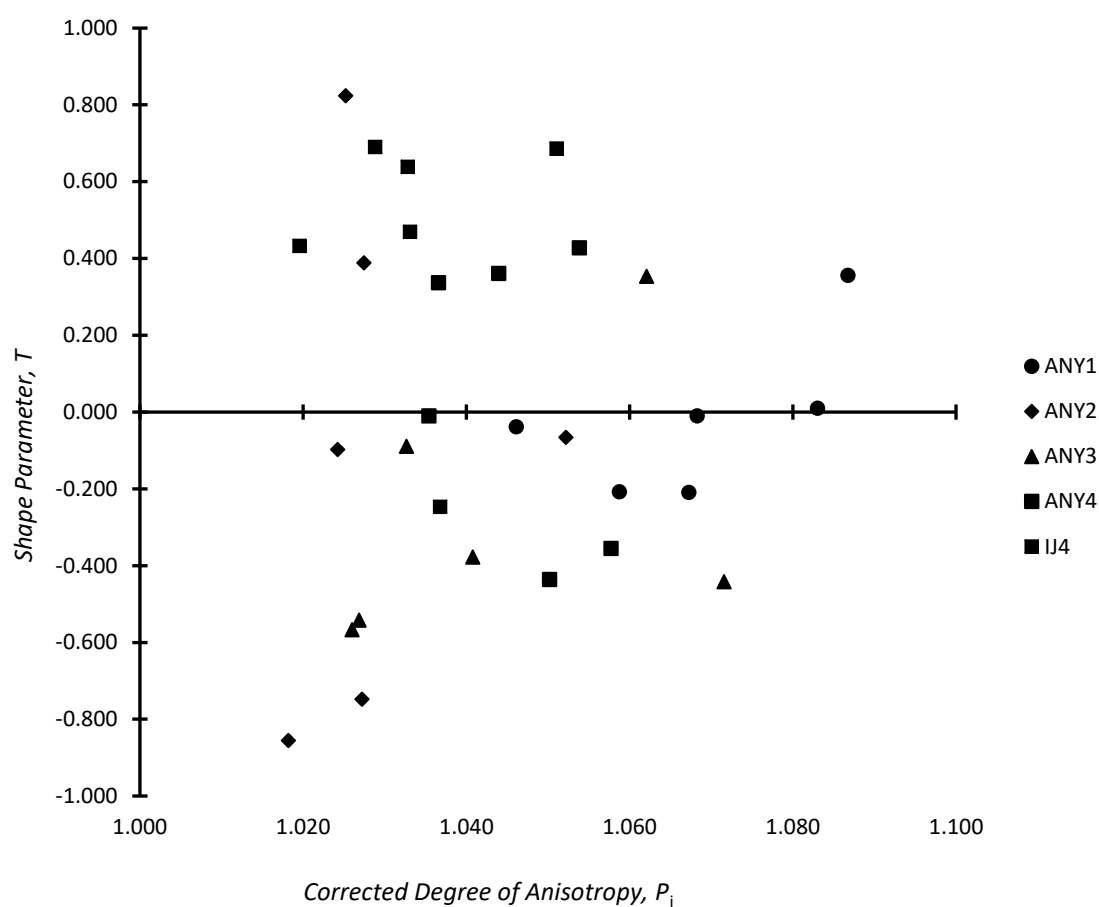


Figure 2. A plot of shape parameter (T) and the corrected degree of anisotropy (P_j). Positive values indicate an oblate shape, whereas negative values indicate a prolate shape.

The degrees of anisotropy for samples used in this study were 1%–8%. These values were typical for basaltic lava flows, which usually less than 10% [5,27,36,37]. Overall, samples from Mt. Anyar had higher degrees of anisotropy on average compared to samples from Mt. Merapi and Mt. Ijen Muda. ANY3 had the highest degree of anisotropy on average. $P\%$ variations between the core samples from the same rock specimen were observed. However, the variations were relatively small.

3.2. Direction of the Principal Susceptibilities

All three axes of susceptibility (K_1 , K_2 , and K_3) were projected onto an equal area stereograph to better represent the declination and inclination of the axes (Figure 3). Mean vectors with their respective circle of confidence calculated using Jelinek statistic [38] gave a statistical insight into the degree of data scatter, represented by the 95% area of confidence (shown as circles of confidences in Figure 3), and how reliably they infer flow direction. The mean values (Table 3) of all principal magnetic susceptibility axes in each sample can be an indication of lava flow direction if the level of confidence of the respective susceptibility axis was high.

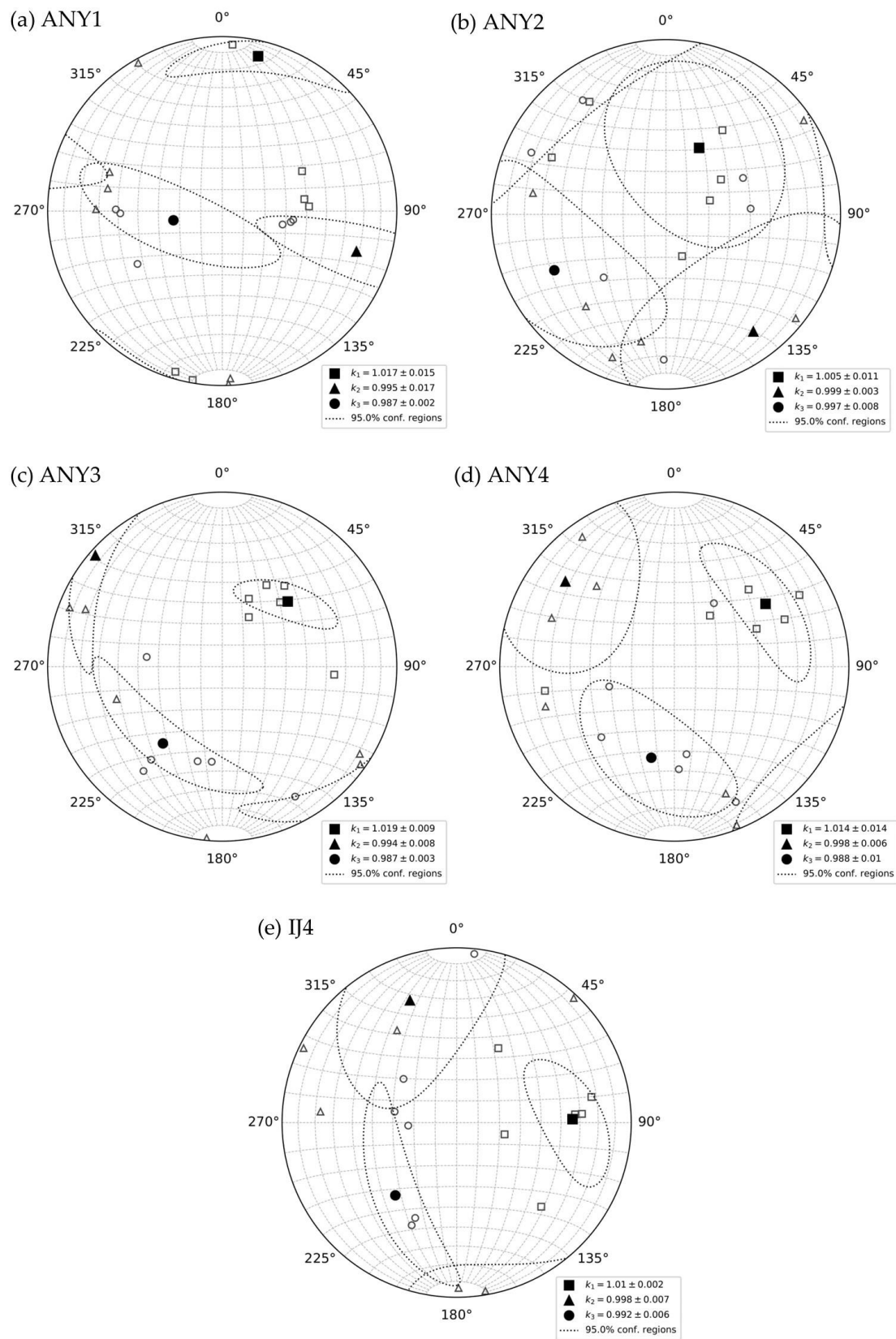


Figure 3. Lower hemisphere projection on equal area stereograph of (a) ANY1; (b) ANY2; (c) ANY3; (d) ANY4 and (e) IJ4 that contain all the principal susceptibilities from six core specimens. Large filled symbols represent the mean vector of each corresponding axis. Circles show the 95% area of confidence. K_1 = maximum susceptibility, K_2 = intermediate susceptibility, and K_3 = minimum susceptibility.

Table 3. Mean values of susceptibility axes of each sample.

Sample	Direction of Mean Principal Susceptibility Axes					
	K ₁		K ₂		K ₃	
	Dec (°)	Inc (°)	Dec (°)	Inc (°)	Dec (°)	Inc (°)
ANY1	13	10	107	21	259	67
ANY2	27	55	143	17	243	29
ANY3	45	46	311	4	218	44
ANY4	55	37	308	22	194	45
IJ4	88	34	339	26	220	45

The maximum axes in all samples generally clustered, except for ANY1 and ANY2, whereas the maximum axes were more scattered and had wider circles of confidence. Intermediate axes were always scattered with shallow inclination or had a low level of confidence. ANY3 and ANY4 had the highest level of confidence for their maximum axes.

3.3. Pore Distribution

Pore distribution images obtained using the micro-computed tomography (μ CT) method are shown in Figure 4. The images show pore distribution cut horizontally (round images) and vertically (rectangular images). The differentiation between the specimen's solid and hollow parts was based on the grayscale filter. We calculated the porosity of each specimen (Table 4) using CTAn software (by Bruker MicroCT, Kontich, Belgium). In accordance with a previous study [31], the result from μ CT and thin-slice showed a very good relationship in the porosity percentage, except for ANY1. However, it was expected given that ANY1 had a low value of porosity. The lower the value of porosity, the calculation of porosity using thin-slice becomes less accurate. The images confirmed the porosity values, where ANY1 and IJ4 had significantly less pore space compared to ANY2, ANY3, and ANY4.

Table 4. Porosity percentage comparison between micro-CT method and thin-slice [25].

Sample	Porosity Percentage	
	μ CT (%)	Thin-Slice (%)
ANY1	1.8	4
ANY2	12.8	12
ANY3	13.4	12
ANY4	15.1	15
IJ4	2.5	2

ANY1 had the lowest percentage of porosity and smallest pore space. This is different from other Mt. Anyar samples (ANY2, ANY3, ANY4), which have a larger pore space. IJ4 fell somewhere in between, despite coming from a different eruption source, which could be caused by the sampling position relative to the lava body. The upper part of a lava flow usually has a larger and higher vesicle density content [39,40].

For specimens, the preferred pore orientations were calculated using the Directionality plugin from ImageJ. We calculated the preferred orientations from the horizontal slices to obtain declination, and from vertical slices to obtain inclination. Vertical slices were cut parallel to the North direction. The preferred orientation and the distribution of pore orientations are better presented with rose diagrams calculated from the directional histograms. The rose diagrams are shown in Figures 5 and 6. The values (Table 5) were calculated by the Directionality plugin.

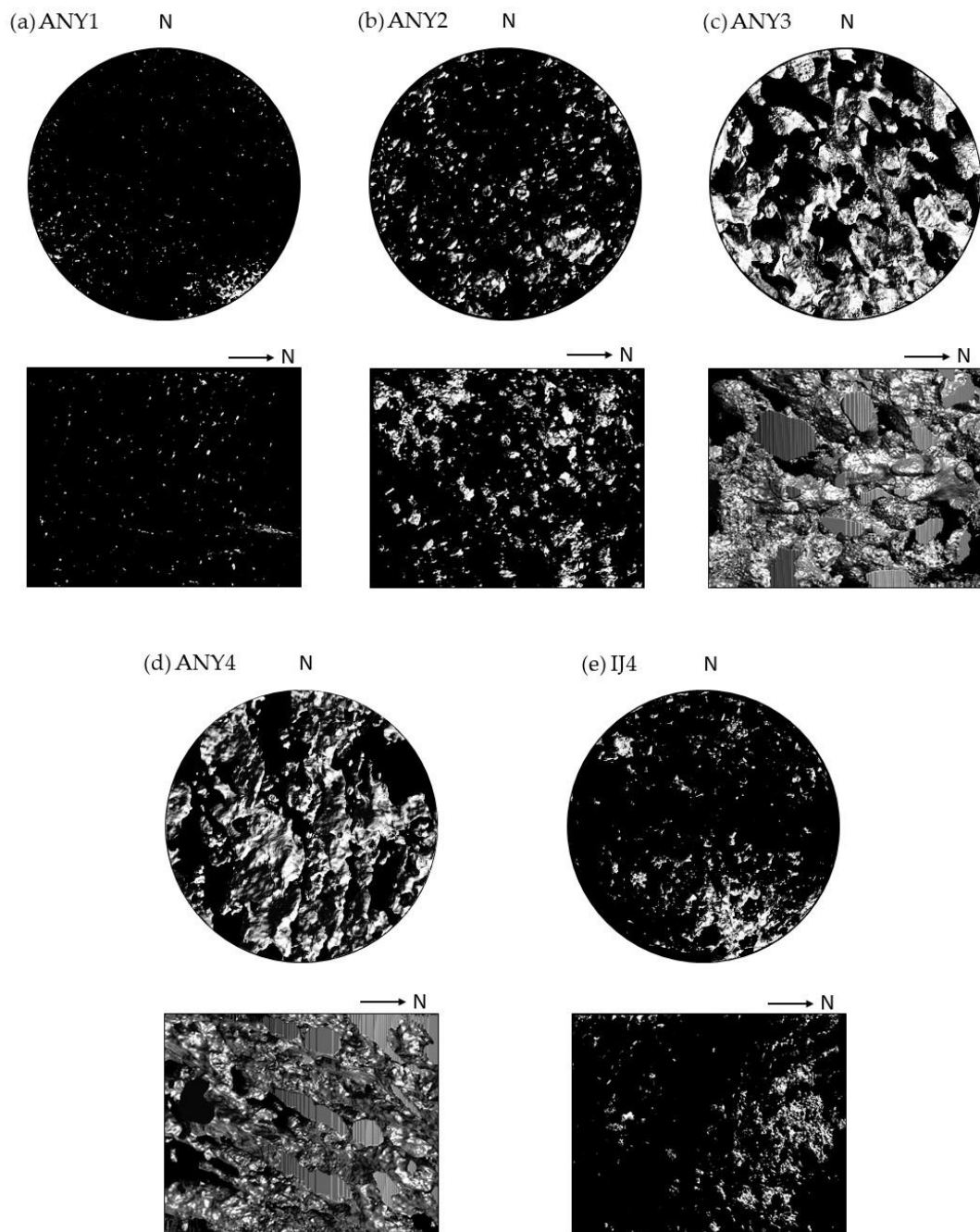


Figure 4. Pore distribution images of (a) ANY1; (b) ANY2; (c) ANY3; (d) ANY4 and (e) IJ4 seen from the top (circles) and side (rectangles) of the core specimens. Black hue represents the solid parts while greyish hue represents the pores. Round images are the vertical view of each sample while rectangular images represent the side view. N indicates north directions. Vertical streaks are from where the pores intersect the scan field. Darker images for ANY1 and IJ4 reflect their relatively low percentage of porosity and small pore space.

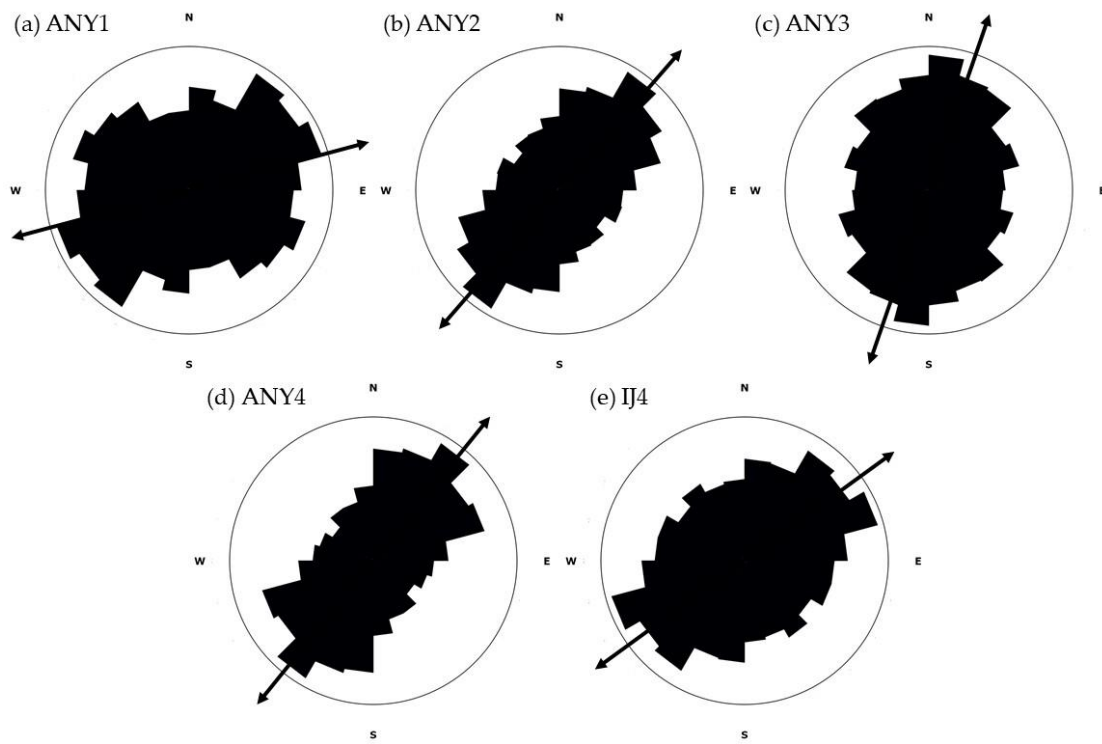


Figure 5. Rose diagrams of horizontal slices of (a) ANY1; (b) ANY2; (c) ANY3; (d) ANY4 and (e) IJ4 specimens that were used in μ CT imaging. These diagrams show the distribution of the declination of pores orientation. Vertical axis represents North-South direction while horizontal axis represents East-West direction. Black arrows indicate the declination preferred pore orientation.

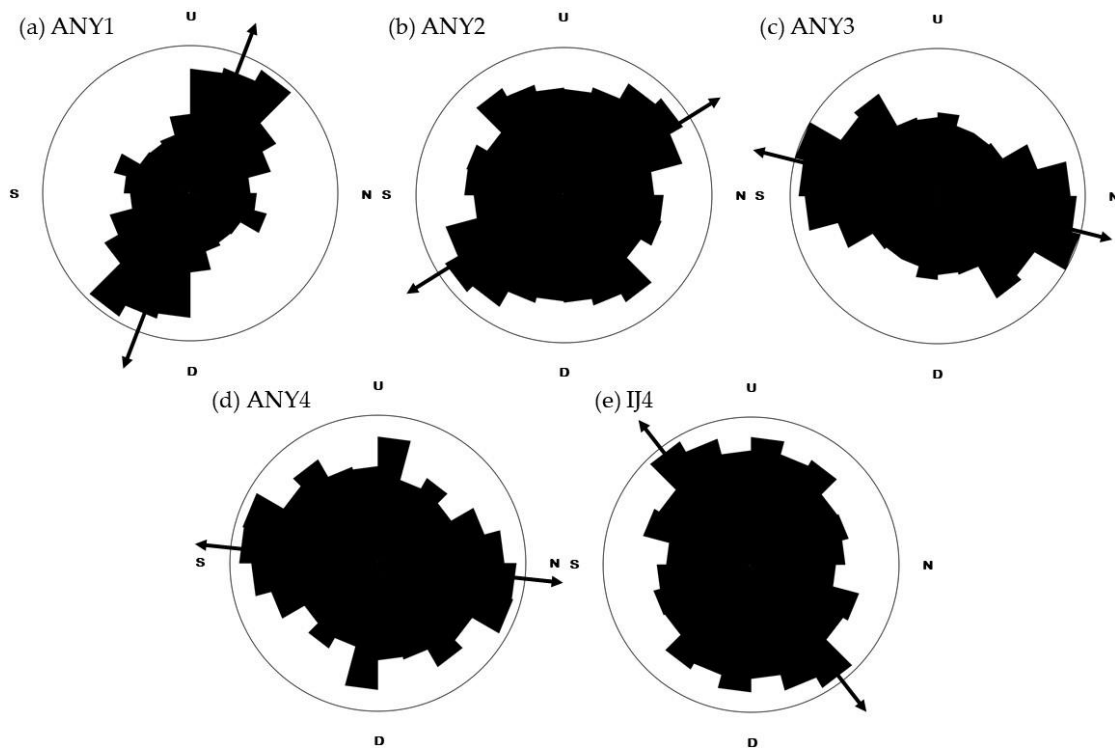


Figure 6. Rose diagrams of vertical slices of (a) ANY1; (b) ANY2; (c) ANY3; (d) ANY4 and (e) IJ4 specimens that were used in μ CT imaging. These diagrams show the distribution of the inclination pores orientation. Vertical axis represents Up-Down direction while horizontal axis represents North-South direction. Black arrows indicate the inclination preferred pore orientation.

Table 5. Preferred pore orientation calculated using the Directionality plugin from ImageJ and the angle between preferred pore orientation and either K_1 , K_2 , or K_3 . * indicates the closest axis to the preferred orientation.

Sample	Preferred Pore Orientation		Angle between Preferred Pore Orientation and Susceptibility Axes		
	Dec (°)	Inc (°)	K_1 (°)	K_2 (°)	K_3 (°)
ANY1	75	69	71	52	46 *
ANY2	41	32	25 *	89	65
ANY3	199	14	64	68	34 *
ANY4	219	6	71	52	46 *
IJ4	234	52	90	78	12 *

4. Discussion

Using AMS to interpret lava flow direction has not always been successful [6–9], however, the implications are undeniable [13]. The most common conclusion is that a specimen with normal fabric will have the maximum axes lay parallel to the flow plane [1–4]. Following this, other studies concluded that the maximum axes would be parallel with the flow plane only if the lava had a laminar flow [41], or it will be parallel to the local lava flow direction [11]. A general geometry of magnetic fabric can be seen in most cases (Figure 3), with ANY3 and ANY4 being the most well-defined, in contrast with ANY1.

Based on the topographical slope, ANY1, ANY2, ANY3, and ANY4 have a relative slope with northeast direction. This confirmed by the maximum susceptibility axes of all samples from Mt. Anyar. On the other hand, IJ4 has a relative slope to the northwest direction while its maximum susceptibility axis has the declination of 88° . In the case of IJ4, the topographical slope is closely parallel to the intermediate susceptibility axis. These conditions are likely related to the magnetic ellipsoid shape of each sample, where samples from Mt. Anyar generally (except ANY4) have prolate shapes (highly influenced by the maximum axis), while the sample from Ijen crater has overall oblate shape.

We investigated the possibility that analyzing pore orientation is reliable enough to support AMS data. Qualitatively, all samples from Mt. Anyar have the direction of the declination of the axis of the preferred pore orientation relative to the northeast-southwest, as shown in Figure 5. This coincides with the direction of topographical slopes and the mean vector of the maximum susceptibility axes. In the case of IJ4, the axis of the preferred pore orientation lays parallel with the maximum susceptibility axis but perpendicular to the topographical slope.

The inclinations of the axes of preferred pore orientation are represented by the rose diagrams shown in Figure 6. In order to determine the actual direction from the axes, we observed the direction of which the inclination is positive (below the north-south axis on the rose diagrams). Based on this, we chose the value of the declination and inclination of preferred pore orientation of each sample and later calculated their correlations with their respective AMS data.

Table 5 shows the calculated preferred pore orientation for each sample. In order to find the correlation between AMS and pore orientation, we calculated the angle between the preferred orientations and all susceptibility axes of each sample using Stereonet program (developed by Richard Allmendinger) [42,43] (Table 5). The axis with the smallest gap to the preferred pore orientation of each sample is assumed to imply the lava flow direction. Following this assumption, it can be observed that the flow directions of ANY2 lay closer to the maximum axes, while it is closer to the minimum axes for ANY1, ANY3, ANY4, and IJ4.

These results are consistent only with the topographical slopes of ANY2. The sample was taken from the lower part of the lava flow, shows good conformity between AMS (respective to the susceptibility axis), preferred pore orientation, and topographical slope. This may be because the lower zone usually has less density and size of vesicles than the upper part. In addition, it usually is the most

indicated region to obtain lava flow direction from AMS [44]. It also should be noted that ANY2 has the lowest average of degree of anisotropy.

In contrast, the results for ANY1, ANY3, and ANY4 show that the preferred pore orientations are not close to the maximum axes, but instead are nearly perpendicular to each other. For both ANY3 and ANY4, despite their relatively good AMS fabric, this can be considered as the effect of larger size and population of pores [45], as ANY3 and ANY4 are both taken from the upper part of the lava flow [41,42]. This could make the distribution of the pore space more ambiguous because the directions are evenly distributed. The software used to determine the pore direction (Directionality plugin from ImageJ) calculates all possible directions of the pores. Therefore, larger size and population tend to make the calculated direction more evenly distributed. In addition, AMS can be disturbed in the upper part of lava with high concentration of vesicles [11], making it more scattered [41].

Considering the topographical slopes of all Mt. Anyar samples, the preferred pore orientations of all samples (Table 5) should be to the northeast direction. Instead, for both ANY3 and ANY4 they are shifted nearly 180 degrees. This suggests that the rock bodies of ANY3 and ANY4 had undergone several geological deformations. As shown in Figure 1, both were taken near a fault line. Thorough examination of both rock bodies is needed for more accurate results.

A different case is observed with IJ4. The result shows that the preferred pore orientation is not consistent with the topographical slope. It is nearly parallel with the minimum susceptibility axis, making it nearly perpendicular to the intermediate and the maximum axes. In this case, all three parameters show no positive correlation. If the assumption of relative sampling position used for ANY2 taken into account, IJ4 should show a good conformity within all parameters. This can be accommodated by considering its magnetic ellipsoid, which are mostly oblate. However, the effect of exact sampling position within the same zone in a lava body and magnetic ellipsoid for both pore orientation and AMS is still not thoroughly defined. Further examination of the vertical position effects within the lava body relative to the orientation of vesicles is needed.

5. Conclusions

Only one out of five samples (ANY2) show good quantitative conformity between AMS data, preferred pore orientation, and topographical slope. Although ANY1 has a relatively large angle between the preferred pore orientation to all susceptibility axes, the relative direction of all parameters is to the northeast-southwest. A different case is observed with both ANY3 and ANY4 where the preferred pore orientations seem to be shifted nearly 180 degrees. The sampling sites were near a fault line, making it possible that the rock bodies had undergone some deformations. In the case of IJ4, all parameters showed no positive correlation. It should be noted that for all samples except ANY2, the preferred pores orientation lay nearly perpendicular to the maximum susceptibility axis. The different results obtained for each sample maybe influenced by the sample's magnetic ellipsoid and the relative vertical position of the sampling site within a single lava flow unit. The upper part usually has bigger size and pore density, which can disturb AMS data and pore/vesicle orientation. Based on the results of this study, it is advisable to take the samples from the lower part of the flow—which usually have sufficient pores and good AMS data—to determine lava flow direction. As can be seen in the cases of ANY3 and ANY4, another important factor to consider in this analysis is the geological condition of the rock bodies, which in the case of this study was the change of rock bodies' orientations, made apparent by the presence of a fault line. Despite the limitations in statistical aspects, the structure and the results of this study are encouraging and shall be explored further.

Author Contributions: F.R.A., R.F.T., and S.B. conceived and designed the experiments; F.R.A., R.F.T., and A.P. collected the samples; F.R.A. and R.F.T. performed the magnetic measurements; F.D.E.L. performed the μ CT measurements; F.R.A., R.F.T., A.P., S.B., N.R.D.W.N., and S.J.F. analyzed the data; and F.R.A. wrote the paper.

Funding: This research was financially funded by Institut Teknologi Bandung, Indonesia.

Acknowledgments: We thank Richard Ketcham for the fruitful discussion we had through e-mail. We also benefited from the Directionality plugin developed by Jean-Yves Tinevez and we are grateful for our discussion on the Image.sc Forum. We also wish to thank three anonymous reviewers for their constructive comments and criticisms on the early version of this manuscript. We greatly appreciate the work of Exneyder A. Montoya-Araque and Ludger O. Suarez-Burgoa in providing the Python script for Jelinek statistic.

Conflicts of Interest: The authors declare no conflict of interest.

References

1. Knight, M.D.; Walker, G.P.L. Magma flow directions in dikes of the Koolau Complex, Oahu, determined from magnetic fabric studies. *J. Geophys. Res. Space Phys.* **1988**, *93*, 4301–4319. [[CrossRef](#)]
2. Panaiotu, C.; Necula, C.; Merezeanu, T.; Panaiotu, A.; Corban, C. Anisotropy of magnetic susceptibility of quaternary lava flows from the east Carpathians. *Rom. Rep. Phys.* **2011**, *63*, 526–534.
3. Shi, C.; Zhu, R.; Liu, Q. Anisotropy of magnetic susceptibility of Hannuoba basalt, northern China: Constraints on the vent position of the lava sequences. *Geophys. Res. Lett.* **2003**, *30*, 38.
4. Herrero-Bervera, E.; Cañón-Tapia, E.; Walker, G.P.; Tanaka, H. Magnetic fabrics study and inferred flow directions of lavas of the Old Pali Road, O’ahu, Hawaii. *J. Volcanol. Geotherm. Res.* **2002**, *118*, 161–171. [[CrossRef](#)]
5. Khan, M.A. The anisotropy of magnetic susceptibility of some igneous and metamorphic rocks. *J. Geophys. Res. Space Phys.* **1962**, *67*, 2873–2885. [[CrossRef](#)]
6. Kolofikova, K.P. Geological interpretation of measurement of magnetic properties of basalts. An example of Chribsky les lava flow of the Velky Roudny volcano (Nizky Jeseník Mts.). *Cas Miner. Geol.* **1976**, *21*, 287–348.
7. Halvorsen, E. The magnetic fabric of some dolerite intrusions, northeast Spitsbergen; implications for the emplacement. *Earth Planet. Sci. Lett.* **1974**, *21*, 127–133. [[CrossRef](#)]
8. Symons, D.T.A. Age and flow direction from magnetic measurements on the historic Aiyansh flow, British Columbia. *J. Geophys. Res. Space Phys.* **1975**, *80*, 2622–2626. [[CrossRef](#)]
9. Wing-Fatt, L.; Stacey, F.D. Magnetic anisotropy of laboratory materials in which magma flow is simulated. *Pure Appl. Geophys. PAGEOPH* **1966**, *64*, 78–80. [[CrossRef](#)]
10. Maggart, T.T. Using anisotropy of magnetic susceptibility to determine the shearing history of a channelized pahoehoe lava flow. In Proceedings of the 29th Annual Keck Research Symposium in Geology, Oberlin, OH, USA, 21–24 April 2016.
11. Cañón-Tapia, E.; Walker, G.P.; Herrero-Bervera, E. Magnetic fabric and flow direction in basaltic Pahoehoe lava of Xitle volcano, Mexico. *J. Volcanol. Geotherm. Res.* **1995**, *65*, 249–263. [[CrossRef](#)]
12. Cañón-Tapia, E. Anisotropy of magnetic susceptibility of lava flows and dykes: A historical account. *Geol. Soc. Lond. Spéc. Publ.* **2004**, *238*, 205–225. [[CrossRef](#)]
13. Cañón-Tapia, E.; Pinkerton, H. The anisotropy of magnetic susceptibility of lava flows: An experimental approach. *J. Volcanol. Geotherm. Res.* **2000**, *98*, 219–233. [[CrossRef](#)]
14. Lockwood, J.P.; Hazlett, R.W. *Volcanoes: Global Perspective*; Wiley-Blackwell: West Sussex, UK, 2010.
15. Peterson, G.L.; Hawkins, J.W. Inclined pipe vesicles as indicators of flow direction in basalts: A critical appraisal. *Bull. Volcanol.* **1971**, *35*, 369–382. [[CrossRef](#)]
16. Waters, A.C. Determining Direction of Flow in Basalts. *Am. J. Sci.* **1960**, *258*, 350–366.
17. Mees, F.; Swennen, R.; Van Geet, M.; Jacobs, P. *Applications of Computed Tomography in the Geosciences, Special Publications*; Geological Society: London, UK, 2003.
18. Cnudde, V.; Masschaele, B.; Dierick, M.; Vlassenbroeck, J.; Van Hoorebeke, L.; Jacobs, P. Recent progress in X-ray CT as a geosciences tool. *Appl. Geochem.* **2006**, *21*, 826–832. [[CrossRef](#)]
19. Kaestner, A.; Lehmann, E.; Stampanoni, M. Imaging and image processing in porous media research. *Adv. Water Resour.* **2008**, *31*, 1174–1187. [[CrossRef](#)]
20. Voorn, M.; Exner, U.; Barnhoorn, A.; Baud, P.; Reuschlé, T. Porosity, permeability and 3D fracture network characterisation of dolomite reservoir rock samples. *J. Petrol. Sci. Eng.* **2014**, *127*, 270–285. [[CrossRef](#)]
21. Ketcham, R.A.; Carlson, W.D. Acquisition, optimization and interpretation of X-ray computed tomographic imagery: Applications to the geosciences. *Comput. Geosci.* **2001**, *27*, 381–400. [[CrossRef](#)]

22. Mao, L.; Shi, P.; Tu, H.; An, L.; Ju, Y.; Hao, N. Porosity Analysis Based on CT Images of Coal Under Uniaxial Loading. *Adv. Comput. Tomogr.* **2012**, *1*, 5–10. [[CrossRef](#)]
23. Cañón-Tapia, E.; Walker, G.P.L.; Herrero-Bervera, E. The internal structure of lava flows—Insights from AMS measurements II: Hawaiian pahoehoe, toothpaste lava and ‘a’ā. *J. Volcanol. Geotherm. Res.* **1997**, *76*, 19–46. [[CrossRef](#)]
24. Pratama, A.; Hafidz, A.; Bijaksana, S.; Abdurrachman, M. Basaltic lava characterization using magnetic susceptibility identification and presence of opaque minerals in Ijen volcanic complex, Banyuwangi, East Java. In Proceedings of the 1st International Geo-Electromagnetic Workshop, West Java, Indonesia, 21–24 February 2017.
25. Pratama, A.; Bijaksana, S.; Abdurrachman, M.; Santoso, N.A. Rock magnetic, petrography, and geochemistry studies of lava at the Ijen Volcanic Complex (IVC), Banyuwangi, East Java, Indonesia. *Geosciences* **2018**, *8*, 183. [[CrossRef](#)]
26. Sujanto, S.M.Z.; Syarifuddin, M.Z.; Sitorus, K. *Geological Map of the Ijen Caldera Complex, East Java*; Volcanology Survey of Indonesia: Bandung, Indonesia, 1988.
27. Girdler, R.W. The Measurement and Computation of Anisotropy of Magnetic Susceptibility of Rocks. *Geophys. J. Int.* **1961**, *5*, 34–44. [[CrossRef](#)]
28. Sudarningsih, S.; Maulana, L.; Bijaksana, S.; Hafidz, A.; Pratama, A.; Widodo, W.; Iskandar, I. Magnetic Characterization of Sand and Boulder Samples from Citarum River and Their Origin. *J. Math. Fundam. Sci.* **2017**, *49*, 116. [[CrossRef](#)]
29. Sudarningsih, S.; Bijaksana, S.; Ramdani, R.; Hafidz, A.; Pratama, A.; Widodo, W.; Iskandar, I.; Dahrin, D.; Fajar, S.J.; Santoso, N.A. Variations in the Concentration of Magnetic Minerals and Heavy Metals in Suspended Sediments from Citarum River and Its Tributaries, West Java, Indonesia. *Geosciences* **2017**, *7*, 66. [[CrossRef](#)]
30. Yan, Z.; Chen, C.; Fan, P.; Wang, M.; Fang, X. Pore Structure Characterization of Ten Typical Rocks in China. *Electron. J. Geotech. Eng.* **2015**, *20*, 479–494.
31. Taud, H.; Martinez-Angeles, R.; Parrot, J.; Hernandez-Escobedo, L. Porosity estimation method by X-ray computed tomography. *J. Pet. Sci. Eng.* **2005**, *47*, 209–217. [[CrossRef](#)]
32. Ketcham, R.A. Computational methods for quantitative analysis of three-dimensional features in geological specimens. *Geosphere* **2005**, *1*, 32. [[CrossRef](#)]
33. Schneider, C.A.; Rasband, W.S.; Eliceiri, K.W. NIH Image to ImageJ: 25 years of image analysis. *Nat. Methods* **2012**, *9*, 671–675. [[CrossRef](#)]
34. Jelinek, V. Characterization of the magnetic fabric of rocks. *Tectonophysics* **1981**, *79*, T63–T67. [[CrossRef](#)]
35. Tarling, H.H.; Hrouda, F. *The Magnetic Anisotropy of Rocks*; Chapman & Hall: London, UK, 1993.
36. Girdler, R.W. Some Preliminary Measurements of Anisotropy of Magnetic Susceptibility of Rocks. *Geophys. J. Int.* **1961**, *5*, 197–206. [[CrossRef](#)]
37. Zananiri, I.; Kondopoulou, D. Anisotropy of Magnetic Susceptibility (AMS) in Volcanic Formations: Theory and Preliminary Results from Recent Volcanics of Broader Aegean. *Bull. Geol. Soc. Greece* **2004**, *36*, 1308–1315. [[CrossRef](#)]
38. Jelinek, V.; Kropáček, V. Statistical processing of anisotropy of magnetic susceptibility measured on groups of specimens. *Stud. Geophys. Geod.* **1978**, *22*, 50–62. [[CrossRef](#)]
39. Caballero-Miranda, C.; Alva-Valdivia, L.; González-Rangel, J.; Gogitchaishvili, A.; Urrutia-Fucugauchi, J.; Kontny, A. Vertical AMS variation within basalt flow profiles from the Xitle volcano (Mexico) as indicator of heterogeneous strain in lava flows. *J. Volcanol. Geotherm. Res.* **2016**, *311*, 9–28. [[CrossRef](#)]
40. Aubele, J.C.; Crumpler, L.; Elston, W.E. Vesicle zonation and vertical structure of basalt flows. *J. Volcanol. Geotherm. Res.* **1988**, *35*, 349–374. [[CrossRef](#)]
41. Macdonald, W.; Palmer, H.; Hayatsu, A. Egan Range Volcanic Complex, Nevada: Geochronology, paleomagnetism and magnetic fabrics. *Phys. Earth Planet. Inter.* **1992**, *74*, 109–126. [[CrossRef](#)]
42. Allmendinger, R.W.; Cardozo, N.C.; Fisher, D. *Structural Geology Algorithms: Vectors Tensors*; Cambridge University Press: Cambridge, UK, 2013.
43. Cardozo, N.; Allmendinger, R.W. Spherical projections with OSXStereonet. *Comput. Geosci.* **2013**, *51*, 193–205. [[CrossRef](#)]

44. Bascou, J.; Camps, P.; Dautria, J.M. Magnetic versus crystallographic fabrics in a basaltic lava flow. *J. Volcanol. Geotherm. Res.* **2005**, *145*, 119–135. [[CrossRef](#)]
45. Sahagian, D.L.; Proussevitch, A.A.; Carlson, W.D. Analysis of Vesicular Basalts and Lava Emplacement Processes for Application as a Paleobarometer/Paleoaltimeter. *J. Geol.* **2002**, *110*, 671–685. [[CrossRef](#)]



© 2019 by the authors. Licensee MDPI, Basel, Switzerland. This article is an open access article distributed under the terms and conditions of the Creative Commons Attribution (CC BY) license (<http://creativecommons.org/licenses/by/4.0/>).